Development of high-coercivity state in high-energy and high-temperature Sm-Co-Fe-Cu-Zr magnets upon step cooling

A.G. Popov[a,b], O.A. Golovnia[a,b,1], V.S. Gaviko[a,b], D.Yu. Vasilenko[c], D.Yu. Bratushev[c], V. I. Nithin Balaji[d], A. Kovács[e], K.G. Pradeep[d], and R. Gopalan[f]

[a]M.N. Miheev Institute of Metal Physics of Ural Branch of Russian Academy of Sciences, Russia, 620990, Ekaterinburg, Str. S. Kovalevskoy, 18

[b]Institute of Natural Sciences and Mathematics, Ural Federal University, Russia, 620002, Ekaterinburg, av. Mira, 19

[c]Ural electromechanical plant, Russia, 620137, Ekaterinburg, Str. Studencheskaya, 137

[d]Department of Metallurgical and Materials Engineering, Indian Institute of Technology Madras, Chennai, India

[e]Ernst Ruska-centre for Microscopy and Spectroscopy with Electrons and Peter Grünberg Institute, Jülich, Germany

[f]International Advanced Research Centre for Powder Metallurgy and New Materials (ARCI), IITM Research Park, Chennai-600113, India

[1]Corresponding author: Tel. +7-343-3783782

E-mail: golovnya@imp.uran.ru

Abstract

The work compares the peculiarities of the high-coercivity state formation in the Sm-Co-Fe-Cu-Zr high-temperature and high-energy permanent magnets (HTPM and HEPM) in the course of the heat treatment with temperature decreasing stepwise from 850 to 400°C. Two types of magnets with varying Fe concentration, i.e., $Sm(Co_{0.88-x}Fe_xCu_{0.09}Zr_{0.03})_7$ with x = 0; 0.04; 0.08; 0.12 (the HTPMs) and $Sm(Co_{0.88-x}Fe_xCu_{0.06}Zr_{0.03})_{7.5}$ with x = 0.24 – 0.33 (the HEPMs) were studied at different temperatures of heat treatment by x-ray diffraction and magnetic analysis, followed by microstructure characterization using transmission electron microscope and near-atomic scale chemical analysis by atom probe tomography. In HEPMs, the main increase in coercivity and relaxation of stresses are observed at high temperatures ($T \approx 700$°C) accompanied by intensive enrichment of the 1:5 phase in Cu. In HTPMs, the coercivity monotonously increases in the entire temperature range of the slow cooling from 700 to 400°C at a rate of 0.5°C/s. At the temperature close to the Curie temperature (~550 °C) of the $Sm(Co,Cu)_5$-type phase, the anomaly of the coercivity increment has been observed. The interphase stresses grow and the elemental redistribution is accelerated simultaneously. The non-uniform Cu distribution in the 1:5 phase can be described by the formation of Cu-rich interlayers at the interface of the $Sm(Co,Cu)_5$ and $Sm_2(Co,Fe)_{17}$-type phases.

Keywords:

Sm-Co-Fe-Cu-Zr

permanent magnet

Sm_2Co_{17}

$SmCo_5$

coercivity kinetics

Atom Probe Tomography

1 Introduction

$Sm(Co_{bal}Fe_xCu_yZr_w)_z$ alloys with the Curie temperature exceeding 800°C [1–3] are excellent materials for high-coercivity permanent magnets, which are suitable for high-temperature applications. The magnets with operating temperature falling in the range from 300 to 550°C are widely applied in devices such as hybrid cars, powerful wind turbines, as well as special aviation equipment [2].

The temperature coefficient coercivity given as, $\beta = dH_c/dT$ of the $Sm(Co_{bal}Fe_xCu_yZr_w)_z$ magnets can significantly vary based on the composition. By the sign and magnitude of β, these magnets can be divided into two types, i.e., the so-called high-temperature (HTPMs) and high-energy permanent magnets (HEPMs). The HTPMs [4–12] are enriched in Sm and Cu, and depleted with Fe ($0<x<0.12$); while on the contrary, the HEPMs have low Sm and Cu ($7.5<z<8.0$ and $0.04<y<0.06$) and high Fe ($0.20<x<0.35$) [13–20] concentrations. Such choice of compositions favors the formation of up to 30–50% and less than 10% of the volume fraction of the $Sm(Co,Cu)_5$ phase in the HTPMs and HEPMs, respectively. The maximum energy product $(BH)_m$ of the HTPMs is approximately 20 MGOe; however, the magnitude of β [21] can be both positive [22,23], zero, and negative in the temperature range below the Curie temperature T_C of the $Sm(Co,Cu)_5$-type phase ($T_C \sim 550$°C). This fact provides the high thermal stability of magnetic hysteresis properties of the HTPMs, whose operating temperature is close to 550°C. $(BH)_{max}$ of the HEPMs can reach up to 35MGOe [18]; however, this group of magnets will have negative β with the approximate value of -0.3%/°C and with the operating temperature not exceeding 300°C. The nanocrystalline cellular structure, which consists of the $Sm_2(Co,Fe)_{17}$ (2:17) cells, the $Sm(Co,Cu)_5$ (1:5) cell-boundary phase, and lamellar Z-phase, emerges after the prolonged annealing of the $Sm(Co_{bal}Fe_xCu_yZr_w)_z$ magnets at about 850°C. However, the hard magnetic state develops as a result of elemental redistribution between the 2:17 and 1:5 phases in the course of the slow cooling from 850 to 400°C. The focus of this work is to compare peculiarities of the high-coercivity state formation in the Sm-Co-Fe-Cu-Zr magnets of the HTPM- and HEPM-type in the course of the heat treatment with stepwise decrease of temperature [24,25].

2 Material and methods

Two types of magnets with various Fe concentration, i.e., $Sm(Co_{0.88-x}Fe_xCu_{0.09}Zr_{0.03})_7$ with x = 0; 0.04; 0.08; 0.12 (the HTPMs) and $Sm(Co_{0.88-x}Fe_xCu_{0.06}Zr_{0.03})_{7.5}$ with $x = 0.24 – 0.33$ (the HEPMs), were prepared by powder metallurgy route. The samples were sintered at temperatures ranging from 1200 to 1215°C. The solid-solution treatment was performed at temperatures from 1200 to 1150°C for $x = 0.24 – 0.33$, respectively. In order to achieve the high-coercivity state, the magnets were subsequently annealed at 830°C for 25 h and then cooled to 400°C at a rate of 0.5ºC/min or with the temperature decreasing stepwise. Hysteresis loops were measured with a vibrating-sample magnetometer, Lakeshore 7404 in magnetic fields up to 17.5 kOe. XRD investigations were carried out using an Empyrean (PANanalytical) diffractometer with Cu-*K*α radiation. The Rietveld refinement was carried out using FULLPROF software. The needle shaped APT specimens were annular milled using dual beam FEI Helios G4 UX focused ion beam/scanning electron microscopy (FIB/SEM). Atom probe tomography (APT) measurements were performed using CAMECA LEAP 5000 XR system in laser mode with a pulse frequency of 200 kHz and 30 pJ laser energy . The data analysis was

performed with the Integrated Visualization and Analysis Software (IVAS 3.8.4) of CAMECA Instruments Inc. TEM information to be included.

3 Results and discussion

Figure 1 demonstrates the dependence of magnetic hysteresis properties of the HTPMs and HEPMs on Fe content. With increasing Fe content, all the magnetic characteristics gradually enhance with the exception of H_c and $(BH)_m$ at x > 0.29. At x > 0.29, the coercivity and $(BH)_m$ decrease abruptly. As discussed above, an increase in the Fe concentration together with decreasing Sm and Cu contents in the HEPMs decreases the volume fraction of the $Sm(Co,Cu)_5$ phase. The electron microscopy study showed that, in the HEPMs with x = 0.33, increased Fe content complicates the formation of the uniform solid solution in the course of the solid-solution treatment, which results in its decomposition during the isothermal annealing at 830°C followed by the irregular microstructure. Figure 2 demonstrates images of the microstructure obtained by TEM. Two different regions several microns in size can be seen, i.e., (1) parallel bands of the 2:17 structure with varying Sm and Cu content, (2) regions with poorly developed cellular structure. The amount of the 1:5 phase in the cellular structure decreases to the limit that it becomes incapable of forming continuous mesh of boundaries around the 2:17 cells.

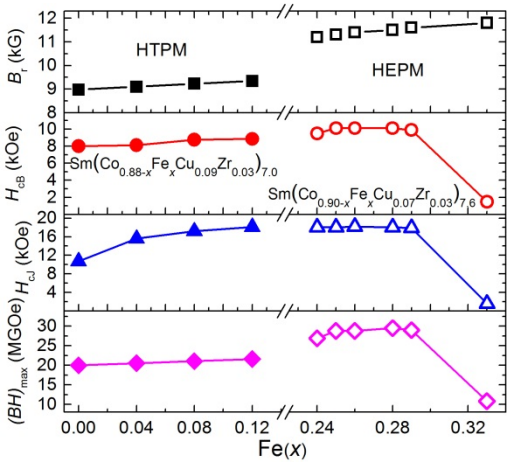

Fig.1. Magnetic properties of the HTPMs and HEPMs

Figures 3 and 4 demonstrates the APT 3-D reconstructions of the $Sm(Co_{0.59}Fe_{0.33}Cu_{0.06}Zr_{0.02})_{7.5}$ magnet, where the Cu distribution is apparently non-uniform, which evidences the discontinuous distribution of the 1:5 phase over the cell boundaries. The concentration profiles Fig. 4 were measured from the cylindrical region, intersecting a Cu-rich phase as shown in Fig. 3. The profiles demonstrate that the magnet is characterized by Cu segregations in the fragments of the 1:5 phase, where the Cu content reaches 50 at %. Thus, the non-uniformity of the cellular structure is the main reason for the observed deterioration of the magnetic properties (Fig. 1).

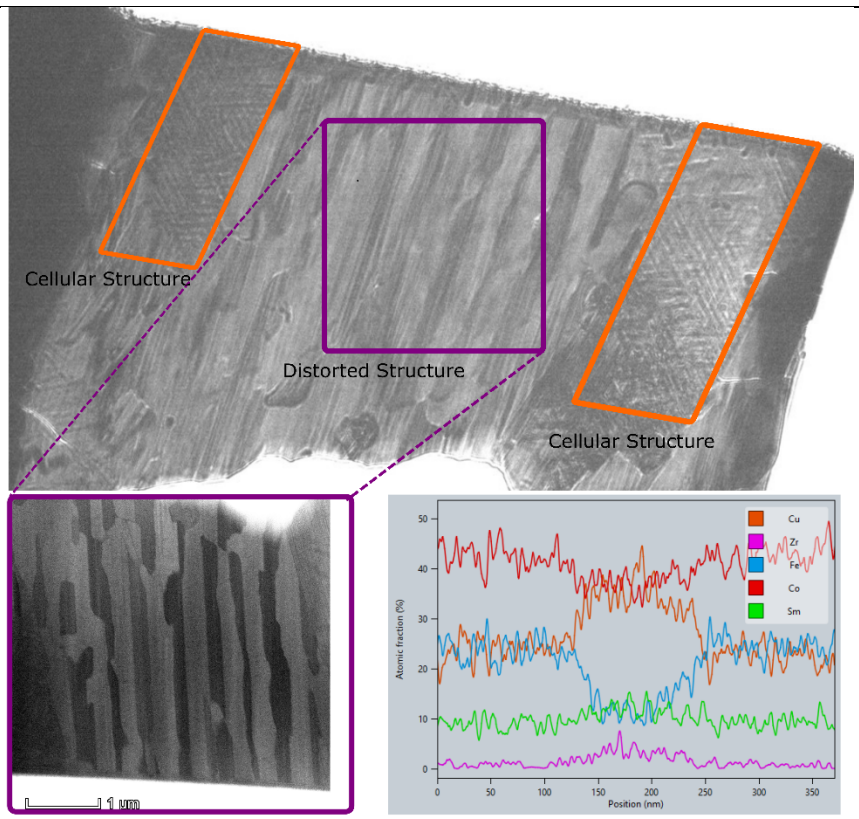

Fig. 2. TEM images of the $Sm(Co_{0.59}Fe_{0.33}Cu_{0.06}Zr_{0.02})_{7.5}$ magnet

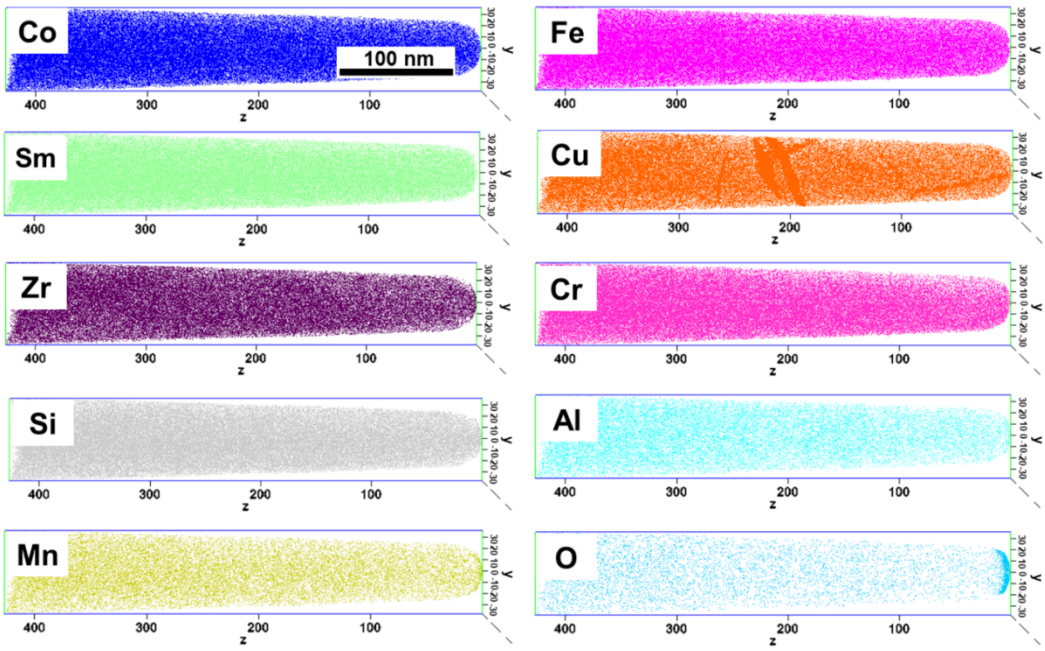

Fig. 3. APT analysis of the $Sm(Co_{0.59}Fe_{0.33}Cu_{0.06}Zr_{0.02})_{7.5}$ magnet showing elemental mapping

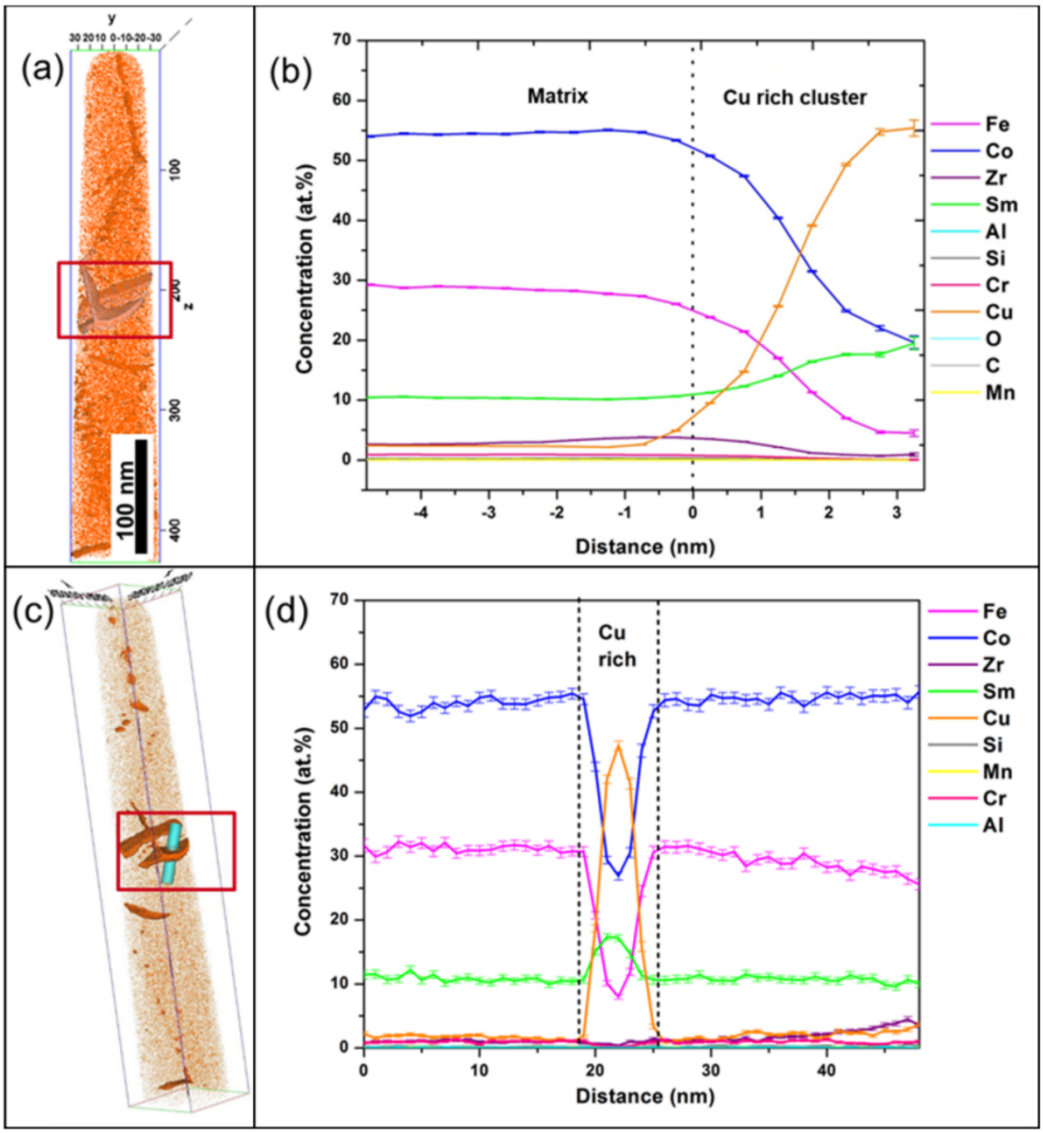

Fig. 4. APT analysis of the $Sm(Co_{0.59}Fe_{0.33}Cu_{0.06}Zr_{0.02})_{7.5}$ magnet showing concentration profiles

Figure 5 demonstrates the coercivity dependences of the $Sm(Co_{0.76}Fe_{0.12}Cu_{0.09}Zr_{0.03})_7$ HTPMs (a) and $Sm(Co_{0.64}Fe_{0.28}Cu_{0.06}Zr_{0.02})_{7.5}$ HEPMs (b) *vs* time of annealing at different steps of the step cooling from 700 to 400°C, respectively. The most substantial increase in coercivity is observed at the initial stages of annealing. In the course of the sufficiently prolonged annealing, the coercivity approaches constant values which increase with decreasing temperature. The temperature dependences of coercivity for the HTPMs and HEPMs are considerably different. In the case of the HTPMs, at 700°C the increase of H_c is found to be rapid, while at 600°C it slows down, it increases abruptly at 500°C, and at 400°C it is the slowest. Upon annealing at 500°C, the anomalous kinetics of the coercivity has been observed. It can be attributed to that the annealing temperature passes through the Curie temperature of the 1:5 phase (near 550°C) and the corresponding accelerated Cu redistribution [12,24,25]. The main increase of H_c in the HEPMs occurs upon annealing at T = 700°C. At T < 700°C, H_c increases negligibly. Figure 5 c summarizes the coercivity development process in the cases of the HEPMs and HTPMs. In the case of the HEPMs, the high annealing temperatures considerably affect the coercivity formation, which is contrary to the case of the HTPMs.

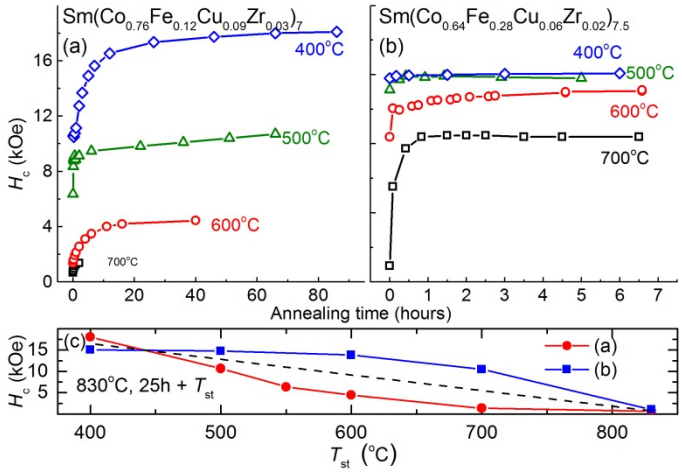

Fig. 5. Coercivity of the $Sm(Co_{0.76}Fe_{0.12}Cu_{0.09}Zr_{0.03})_7$ (the HTPMs) (a) and $Sm(Co_{0.64}Fe_{0.28}Cu_{0.06}Zr_{0.02})_{7.5}$ (the HEPMs) (b) *vs.* time and temperature (c) of annealing at different steps of the step cooling

Figures 6 shows fragments of XRD patterns taken from the planes perpendicular to the texture direction of the magnets (HTPMs (Fig. 6a) and HEPMs (Fig. 6b)) after quenching from 830°C and after step annealing at 700, 500 and 400°C. The volume fraction of the $Sm(Co,Cu)_5$ phase in the HTPMs quenched from 830°C reaches 50% (Table 1); and the difference in the *c* lattice parameters of the $Sm_2(Co,Fe)_{17}$ and $Sm(Co,Cu)_5$ phases is negligibly small (Fig. 6a). Therefore, the Cu redistribution at T = 700 and 600°C is slow and insignificant, so that it cannot considerably contribute to the increase of H_c. Since the Curie temperature of the 1:5 phase $T_C^{1:5}$ is approximately 550°C, after decreasing the annealing temperature to 500°C, the 1:5 phase becomes ferromagnetic and a strong magnetovolume effect is observed [12,24,25], which manifests in large change in the crystal lattice parameters (Fig. 6 a). The 1:5 phase shrinks along the *c* axis, which increases the misfits with 2:17 phase and interphase stresses. The uphill diffusion of Cu to the 2:17/1:5 interface efficiently relaxes interphase stresses. Thus, at this temperature, a considerable acceleration of the Cu diffusion and increase of H_c are observed (Fig. 5a). Especially, this is true for the initial step of annealing (t < 0.2 h).

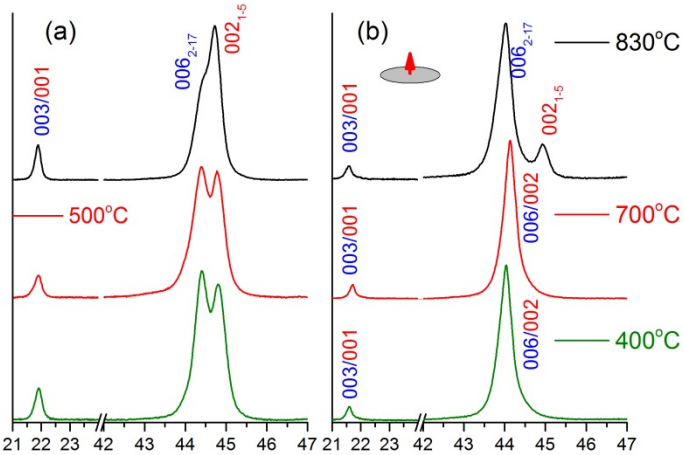

Fig. 6. Fragments of XRD patterns taken from the planes perpendicular to the texture direction of the HTPMs (a) $(Sm(Co_{0.76}Fe_{0.12}Cu_{0.09}Zr_{0.03})_7)$ and HEPMs (b) $(Sm(Co_{0.64}Fe_{0.28}Cu_{0.06}Zr_{0.02})_{7.5})$ after quenching from 830, 700, 500, and 400°C

Table 1. Phase composition and lattice parameters of the HTPMs and HEPMs before and after slow cooling.

	$Sm(Co_{0.76}Fe_{0.12}Cu_{0.09}Zr_{0.03})_7$	$Sm(Co_{0.6}Fe_{0.28}Cu_{0.06}Zr_{0.03})_{7.5}$

Phase	830°C 25h					
	Fract (%)	*a*, Å	*c*, Å	Fract (%)	*a*, Å	*c*, Å
2:17	51	8.4671	12.2103	77	8.4847	12.3255
1:5-I	37	4.9548	4.0371	19	4.9563	4.06
1:5-II	13	4.9319	4.0409	4	4.9023	3.8841
	850°C 25h + 800°C 20min +SC					
2:17	59	8.4620	12.2188	89	8.4864	12.3248
1:5-I	33	4.9660	4.0347	7	4.9835	4.0745
1:5-II	9	4.9245	4.0372	4	4.9369	3.8682

In order to understand how Cu relaxes the stresses, it is necessary to analyze carefully the powder diffraction patterns. Figure 7 demonstrates the powder diffraction patterns of the HTPMs and HEPMs before and after the step annealing. After quenching of the HTPMs from 830°C, the (110) and (020) reflections of the 1:5 phase are smeared. Thus, it cannot be fitted by only one spectrum. Such patterns can originate from the 1:5 phase that forms thin stressed interlayers with continuous Cu distribution. After the step annealing total weight fraction of the $Sm(Co,Cu)_5$ phase decreases from 50 to 42%. Since in the course of step annealing the 1:5 phase becomes enriched in Cu, a decrease in its fraction can only occur due to its intensive depletion with Fe and Co. Thus, the 1:5 phase should also enrich in Sm, and, consequently, approach the stoichiometric composition. In addition, after the step annealing, the relative shift of the two subspectra of the 1:5 phase increases. This can be attributed to the formation of the interlayers at the interface of the 1:5 and 2:17 phases. It can be assumed that one subspectrum corresponds to the Cu-rich phase and another to the 1:5 phase depleted with Cu. The Cu-enrichment at the interface between the 2:17 and 1:5 phases relaxes the stresses and increases the boundary-energy gradient, as well as H_c.

As can be seen from Table 1, in the case of the HEPMs, after the step cooling, the total weight fraction of the 1:5 phase decreases from 23 to 13%. Quenching from 830°C results in a large misfit of the *c* lattice parameters of the coherent 2:17 and 1:5 phases (Fig. 6b), and, therefore, causes increased misfits at the 2:17/1:5 interface. Taking into account that at the 2:17/1:5 interphase the phases with less difference between the *c*/*a* ratios should be localized, the 1:5-I phase should be the interlayer in the case of the HEPMs. As can be seen from Figs. 5 and 6, main elemental redistribution between the phases and increase in H_c occurs upon annealing at T = 700°C. Generally, these processes are similar to the ones in the case of the HTPMs, i.e., both the 1:5-I and 1:5-II phases become enriched in Cu, which is accompanied by depletion with Fe and Co, so that the composition of both 1:5 phases approach the stoichiometric one. In the course of annealing at T = 700°C, the Cu diffusion from the 2:17 phase into the 1:5 phase leads to the relaxation of the stresses. At T < 700ºC, no change in the XRD patterns has been observed, which explains the negligible increase of H_c (Fig. 5).

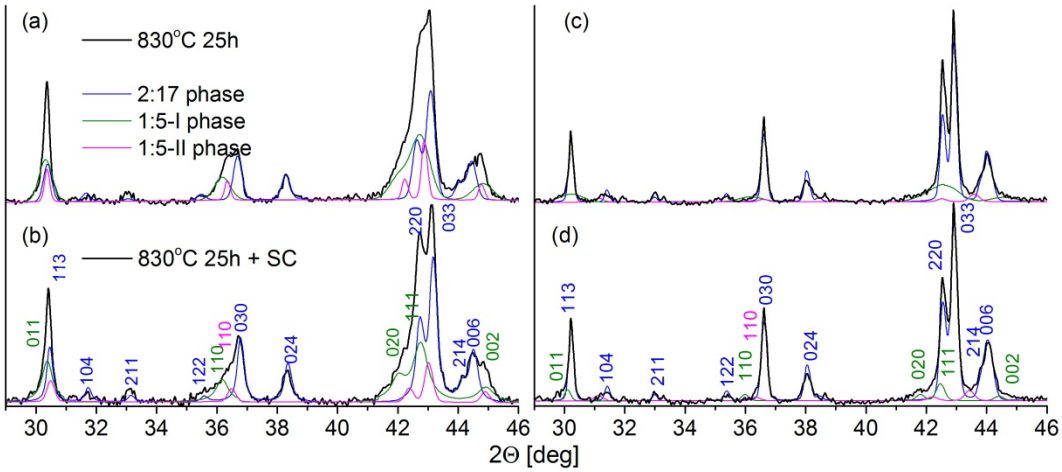

Fig. 7. Fragments of powder XRD patterns of HTPMs (a,b) ($Sm(Co_{0.76}Fe_{0.12}Cu_{0.09}Zr_{0.03})_7$) and HEPMs (c,d) ($Sm(Co_{0.64}Fe_{0.28}Cu_{0.06}Zr_{0.02})_{7.5}$) quenched after various treatments

4 Conclusion

It is demonstrated that the interphase misfits and stresses significantly affect the redistribution of the elements between the 2:17 and 1:5 phases and, hence, the coercivity. In the course of slow cooling, in the HTPMs and HEPMs, the coercivity and stresses develop according to two different schemes.

1) In HEPMs, the main increase in coercivity and relaxation of stresses are observed at high temperatures ($T \approx 700$°C). At the same time, the 1:5 phase intensively enriches in Cu.

2) In HTPMs, the coercivity monotonously increases in the entire temperature range of the slow cooling from 700 to 400°C. In this case, the lower the temperature of annealing, the higher the increase in coercivity. At the temperature close to the Curie temperature of the 1:5 phase (approximately 500°C), the anomaly of the coercivity increment is observed. The interphase stresses grow and the element redistribution is accelerated. The Cu distribution in the 1:5 phase is found to be non-uniform, and, probably, the Cu-rich interlayers are formed at the interface of the 1:5 and 2:17 phases.

Acknowledgements

The research was supported by BRICS STI Framework Program for [RFBR-BRICS project No. 17-52-80072 and DST-BRICS under Proposal 258]. The X-ray diffraction investigation and the magnetic measurements have been performed in the Center of Collaborative Access of IMP UB RAS.

References

[1] M. Duerrschnabel, M. Yi, K. Uestuener, M. Liesegang, M. Katter, H.J. Kleebe, B. Xu, O. Gutfleisch, L. Molina-Luna, Atomic structure and domain wall pinning in samarium-cobalt-based permanent magnets, Nat. Commun. 8 (2017) 1–7. doi:10.1038/s41467-017-00059-9.

[2] J.P. Liu, E. Fullerton, O. Gutfleisch, D.J. Sellmyer, eds., Nanoscale Magnetic Materials and Applications, Springer Science+Business Media, New York, 2009.

[3] T. Ojima, S. Tomizawa, T. Yoneyama, T. Hori, Magnetic properties of a new type of rare-earth cobalt magnets Sm2(Co,Cu,Fe,M)17, IEEE Trans. Magn. MAG-13 (1977) 1317–1319.

[4] H. Sepehri-Amin, J. Thielsch, J. Fischbacher, T. Ohkubo, T. Schrefl, O. Gutfleisch, K. Hono, Correlation of microchemistry of cell boundary phase and interface structure to the coercivity of Sm(Co0.784Fe0.100Cu0.088Zr0.028)7.19 sintered magnets, Acta Mater. 126 (2017) 1–10. doi:10.1016/j.actamat.2016.12.050.

[5] R. Gopalan, K. Hono, A. Yan, O. Gutfleisch, Direct evidence for Cu concentration variation and its correlation to coercivity in Sm (Co0.74Fe0.1Cu0.12Zr. 04)7.4 ribbons, Scr. Mater. 60 (2009) 764–767.

[6] M.S. Walmer, C.H. Chen, M.H. Walmer, A new class of Sm-TM magnets for operating temperatures up to 550°C, in: IEEE Trans. Magn., 2000. doi:10.1109/20.908807.

[7] C.H. Chen, M.S. Walmer, M.H. Walmer, J. Liu, S. Liu, G.E. Kuh, Magnetic pinning strength for the new Sm-TM magnetic materials for use up to 550C, J. Appl. Phys. 87 (2000) 6719–6721.

[8] L. Liu, Z. Liu, M. Li, D. Lee, R.J. Chen, J. Liu, W. Li, A.R. Yan, Positive temperature coefficient of coercivity in Sm1-xDyx(Co0.695Fe0.2Cu0.08Zr0.025)7.2 magnets with spin-reorientation-transition cell boundary phases, Appl. Phys. Lett. 106 (2015) 052408. doi:10.1063/1.4907640.

[9] N. Yu, M. Zhu, Y. Fang, L. Song, W. Sun, K. Song, Q. Wang, W. Li, The microstructure and magnetic characteristics of Sm(CobalFe0.1Cu0.09Zr0.03)7.24 high temperature permanent magnets, Scr. Mater. 132 (2017) 44–48. doi:10.1016/j.scriptamat.2017.01.026.

[10] N. Yu, M. Zhu, L. Song, Y. Fang, K.K. Song, Q. Wang, W. Li, Coercivity temperature dependence of Sm2Co17-type sintered magnets with different cell and cell boundary microchemistry, J. Magn. Magn. Mater. 452 (2018) 272–277. doi:10.1016/j.jmmm.2017.12.058.

[11] T.L. Zhang, Q. Song, H. Wang, J.M. Wang, J.H. Liu, C.B. Jiang, Effects of solution temperature and Cu content on the properties and microstructure of 2:17-type SmCo magnets, J. Alloys Compd. 735 (2018) 1971–1976. doi:10.1016/j.jallcom.2017.11.009.

[12] A.G. Popov, V.S. Gaviko, V. V Popov, O.A. Golovnia, A. V Protasov, E.G. Gerasimov, A. V Ogurtsov, M.K. Sharin, R. Gopalan, Structure and magnetic properties of heat-resistant Sm(Co0.796-xFe0.177CuxZr0.027)6.63 permanent magnets with high coercivity, JOM. 71 (2019) 559–566. doi:10.1007/s11837-018-3240-2.

[13] Y.Q. Wang, Z.F. Shang, M. Yue, D. Wu, D.T. Zhang, H.G. Zhang, W.Q. Liu, Correlation between Fe content and z value in Sm(Co bal Fe x Cu 0.06 Zr 0.025) z permanent magnets, J. Magn. Magn. Mater. 474 (2019) 417–423. doi:10.1016/j.jmmm.2018.11.008.

[14] X.. Y. Xiong, T. Ohkubo, T. Koyama, K. Ohashi, Y. Tawara, K. Hono, The microstructure of sintered Sm(Co0.72Fe0.20Cu0.055Zr0.025)7.5 permanent magnet studied by atom probe, Acta Mater. 52 (2004) 737–748. doi:10.1016/j.actamat.2003.10.015.

[15] K. Song, W. Sun, Y. Fang, S. Wang, N. Yu, M. Zhang, M. Zhu, W. Li, Optimization of microstructures and magnetic properties of Sm(CobalFe0.227Cu0.07Zr0.023)7.6 magnets by sintering treatment, J. Rare Earths. 37 (2019) 171–177. doi:10.1016/j.jre.2018.04.014.

[16] B.M. Ma, Y.L. Liang, J. Patel, D. Scott, C. Bounds, The effect of Fe content on the temperature dependent magnetic properties of Sm(Co,Fe,Cu,Zr)z and SmCo5 sintered magnets at 450oC, IEEE Trans. Magn. 32 (1996) 4377–4379. doi:10.1109/20.538874.

[17] Y. Horiuchi, M. Hagiwara, K. Okamoto, T. Kobayashi, M. Endo, T. Kobayashi, N. Sanada, S. Sakurada, Effect of pre-aging treatment on the microstructure and magnetic properties of Sm (Co, Fe, Cu, Zr) 7.8 sintered magnets, Mater. Trans. 55 (2014) 482–488.

[18] Y. Horiuchi, M. Hagiwara, M. Endo, N. Sanada, S. Sakurada, Influence of intermediate-heat treatment on the structure and magnetic properties of iron-rich Sm(CoFeCuZr)Z sintered magnets, J. Appl. Phys. 117 (2015) 117C704. doi:10.1063/1.4906757.

[19] K. Song, W. Sun, H. Chen, N. Yu, Y. Fang, M. Zhu, W. Li, Revealing on metallurgical behavior of iron-rich Sm(Co0.65Fe0.26Cu0.07Zr0.02)7.8 sintered magnets, AIP Adv. 7 (2017) 056238. doi:10.1063/1.4978464.

[20] H. Chen, Y. Wang, Y. Yao, J. Qu, F. Yun, Y. Li, S.P. Ringer, M. Yue, R. Zheng, Attractive-domain-wall-pinning controlled Sm-Co magnets overcome the coercivity-remanence trade-off, Acta Mater. 164 (2019) 196–206. doi:10.1016/j.actamat.2018.10.046.

[21] H. Kronmüller, D. Goll, Analysis of the temperature dependence of the coercive field of Sm2Co17 based magnets, Scr. Mater. 48 (2003) 833–838. doi:10.1016/S1359-6462(02)00619-X.

[22] A.G. Popov, A. V Korolev, N.N. Shchegoleva, Temperature dependence of the coercive force of Sm (Co, Fe, Cu, Zr) 7.3 alloys, Phys. Met. Metallogr. 69 (1990) 100–106.

[23] A.M. Gabay, W. Tang, Y. Zhang, G.C. Hadjipanayis, Anomalous temperature dependence of coercivity and reversal mechanism in bulk-hardened rare earth-cobalt magnets, Appl. Phys. Lett. (2001). doi:10.1063/1.1354670.

[24] A.G. Popov, O.A. Golovnia, A. V Protasov, V.S. Gaviko, D.A. Kolodkin, R. Gopalan, Coercivity kinetics upon step cooling of the sintered, Rare Earths. (2019).

[25] A.G. Popov, O.A. Golovnia, A. V. Protasov, V.S. Gaviko, R. Gopalan, C. Jiang, T. Zhang, Peculiar kinetics of coercivity of sintered Sm(Co0.78Fe0.10Cu0.10Zr0.02)7 magnet upon slow cooling, IEEE Trans. Magn. 54 (2018) 2100907. doi:10.1109/TMAG.2018.2811369.